Treatment with 188Re Reduces Cancerous Phenotype in Liver Cancer Cells

Samieh Asadian
Royan Institute for Stem Cell Biology and Technology
Abbas Piryaei
Shahid Beheshti University of Medical Sciences
Nematolah Gheibi (gheibi_n@yahoo.com)
Qazvin University of Medical Sciences
Bagher Aziz Kalantari
Islamic Azad University
Mohamad Reza Davarpanah
Shahid Beheshti University
Samaneh Saberi
Pasteur Institute of Iran
Mehdi Azad
Qazvin University of Medical Sciences
Valentina Kapustina
Sechenov University
Sahar Moghbeli Nejad
Qazvin University of Medical Sciences
Morteza Mohamadi
University of Tehran
Anastasia Shpichka
Sechenov University
Peter Timashev (timashev.peter@gmail.com)
Pervyj Moskovskij gosudarstvennyj medicinskij universitet imeni I M Secenova https://orcid.org/0000-0001-7773-2435
Moustapha Hassan
Karolinska Institutet
Massoud Vosough (masvos@Royaninstitute.org)
Royan Institute for Stem Cell Biology and Technology

Research

Keywords: Hepatocarcinoma, Apoptosis, Cell cycle arrest, Rhenium-188 (188Re), radionuclide therapy

Posted Date: April 22nd, 2021

DOI: https://doi.org/10.21203/rs.3.rs-398524/v1

Abstract

Background

Recurrence in hepatocellular carcinoma (HCC) after conventional treatments is a big challenge. Despite the promising progress in advanced targeted therapies, HCC is the fourth leading cause of cancer death worldwide. Radionuclide therapy could be an effective targeted approach to address this concern. Rhenium-188 (^{188}Re) is a β-emitting radionuclide that can be used in clinic for apoptosis induction and inhibit cell proliferation. Although adherent cell cultures are efficient and reliable, the lack of appropriate cell-cell and cell-ECM contact exists. It has been demonstrated that three-dimensional organotypic human cancer models are suitable alternatives.

Methods

Conventional adherent culture and 3D constructs of Huh7 or HepG2 hepatoma cell lines cultured on liver extracellular matrix (ECM) were treated by different doses of ^{188} Rhenium Perrhenate ($^{188}ReO_4$). To evaluate cell viability, live/dead assay carried out. The flow-cytometric assay, qRT-PCR, western bolting, colony formation assay, and immunofluorescence (IF) studies were performed to investigate the therapeutic effect of $^{188}ReO_4$. Subsequently, the tumor formation ability of $^{188}ReO_4$-treated Huh7 cells was evaluated in animal model.

Results

According to viability assay and live/dead staining, the number of dead cells in Huh7 and HepG2 lines were significantly increased compared to untreated control groups. Data obtained from Annexin/PI showed that Huh7 and HepG2 cells showed typical apoptotic changes after treatment with $^{188}ReO_4$. Quantitative RT-PCR and western blotting data also supported that $^{188}ReO_4$ treatment can induce apoptosis. Furthermore, cell cycle arrest observed in G2 phase after exposure to effective dose of $^{188}ReO_4$ in Huh7 cells. Colony formation assay confirmed growth suppression in Huh7 and HepG2 cells post exposure. The IF also displayed proliferation inhibition in the $^{188}ReO_4$ treated cells on 3D scaffolds of liver extracellular matrix (LEM). In 2D culture, PI3-AKT signaling pathway remained unchanged whereas, in the 3D condition it was activated. Treated Huh7 cells with effective dose of $^{188}ReO_4$ lose their tumor formation ability in nude mice compare to the control group.

Conclusion

The results supported that $^{188}ReO_4$ could induce apoptosis and cell cycle arrest and inhibit tumor formation capacity in HCC cells.

Introduction

Hepatocellular carcinoma (HCC) is the dominant variety of liver cancers, represents the sixth prevalent and fourth leading cause of cancer deaths worldwide (1, 2). The main risk factors for HCC are chronic infection with hepatitis C virus (HCV) or hepatitis B virus (HBV), aflatoxin-contaminated foods, alcohol abuse, obesity, smoking, and type 2 diabetes (1, 3). Staging of HCC is vital for prediction of survival and choosing a proper treatment strategy. therapeutic strategies such as hepatectomy, hepatic artery ligation and catheterization, transarterial chemoembolization (TACE), multi-kinases inhibitors (Sorafenib), and external radiation therapy may result in tumor down staging (4, 5). Potentially curative therapy like liver transplantation or surgical resection of tumor might be possible for less advanced HCC (3). After resection, metastasis and recurrence frequently happen and fail the overall survival. In patients with unresectable HCC and preserved liver function, TACE can prolong survival. However, TACE is rarely curative (6). Due to partially benefits of current chemotherapy, or alternative medicine; novel treatments for liver cancer, specially advanced HCC, are in urgent need (6).

Selective radionuclide therapy is an effective local method for the treatment of HCC; this therapy includes Yttrium-90 microspheres (7, 8), Iodine-131 monoclonal antibody (9), and radioactive lipiodol (10). Radioisotopes that continuously emit β-rays can destruct the tumor cells by frequent low-dose radiation after intra tumoral injection (5). Rhenium-188 (^{188}Re) is an easy-available generator-derived radioisotope for therapeutic application that emitting β-particles (2.12 MeV, 71.1% and 1.965 MeV, 25.6%) and image-able gammas (155 keV, 15.1%) (11, 12). Rhenium-188 has been used for the preparation of therapeutic radiopharmaceuticals for the management of different diseases such as bone metastasis, rheumatoid arthritis and primary cancers (13).

The activity of anticancer drugs has been evaluated on two-dimensional (2D) cultured cancer cell lines. However, 2D cell cultures have provided great insight into the ability of tumor cells to grow, but they do not provide information about the complex interactions between the cancer cells and their microenvironment (14–18). This could result in misguided translation of experimental data in 2D condition. The 3D culture systems have received attention as a proper platform to avoid certain drawbacks by recapitulating the tumor microenvironment. It was shown that 3D organotypic human cancer cell models as well as hepatocyte 3D constructs are suitable alternatives models for study and generated data is more valid compare to conventional adherent cultures (19–21). They can be tailored to be biomimetic and accurately recapitulate the native *in vivo*. For example, rat hepatocytes in 3D cultures possess structural polarity and channels with great similarity in structure and function to bile canaliculi, which can explain their enhanced hepatocellular activities (21–23). In contrast to normal cells, tumor cells with stem cell features such as EpCAM + human HCC cells, can also generate 3D spheroids (24).

Here, we have investigated the ^{188} ReO_4 effects on inhibition of cancer development in malignant HCC cells including Huh7 and HepG2. A large panel of HCC cell lines with different mutational profiles would cover a great portion of genomic heterogeneity of primary HCCs. Careful selection would determine

whether these cell lines mimic responses of primary HCCs to different drugs and may lead to a powerful cell line-based platform for precise treatment of HCCs.

Single and double DNA break stimulation results in activation of apoptosis or cell cycle arrest as a part of a negative feedback response to limit proliferation (25, 26). Thus, β − particles irradiation in 2D, 3D, and mouse model results in DNA damage (27–29). Enhanced apoptosis signaling in *in-vitro* and *in-vivo* appears to be a consequence of both increased single and double strand DNA break due to accumulation of therapeutic radionuclide. This has a positive effect to destroy cancerous cells (30, 31). Activation of p53 and BAX following exposure to β − emittion is mediated by DNA damage and apoptosis induction (32–37). However, the effects of ^{188} ReO_4 on apoptosis and cell cycle arrest on the *in vitro* and *in vivo* growth of cancerous HCC cells have not been well studied.

The 3D cell culture systems are based on matrices from natural materials, such as alginate, collagen, and glycosaminoglycan or synthetic sources, such as polyethylene glycol and polyacrylic acid (38–40). Recently, decelluarized extracellular matrix (ECM) derived materials are extensively used in the fields of tissue engineering and regenerative medicine. These materials usually preserve the original composition and partial structure of tissue specific ECM (41, 42).

Recently, researchers successfully used decelluarized ECM materials to develop 3D cancer models (43, 44). Therefore, culturing HCC cells on decelluarized liver extracellular matrix (LEM) might provide a better biomimetic microenvironment for them. In this study, we cultured the Huh7 and HepG2 hepatic cell lines on 3D scaffolds derived from liver-ECM (LEM) hydrogel and called Huh7/HepG2-LEM. To investigate the effect of ^{188} ReO_4 we focused on PTEN/PI3K/AKT signaling pathway to demonstrate that if ^{188} ReO_4 affect radio resistance in the *in vitro* models. In this study our results demonstrate that ^{188} ReO_4 can be a potential new therapeutic agent for HCC. This approach can be combined effectively with antibodies and peptides for more selective and personalized therapy.

Material And Methods

Cell culture. The liver HCC cell lines, Huh7 and HepG2, and the human dermal fibroblast (HDF) were obtained from Royan Cell Bank. The cells were cultured in high-glucose Dulbecco's modified Eagle's medium (HGDMEM, Gibco, 11995-040) media at 37°C in a humidified incubator with 5% CO2. The culture medium was supplemented with 10% fetal bovine serum (FBS, Gibco, 16140-071), 2 mM L-glutamine (Gibco; 25030-024), 1 mM non-essential amino acids (Gibco; 11140-035) and 1% penicillin/streptomycin (Pen/Strep, Gibco; 15070-063, Gaithersburg, MD). Huh7, HepG2, and HDF were sub-cultured by trypsin/EDTA (0.25%, Gibco; 25200056). The culture media were changed every other day.

Generation of HCC-LEM. Because of providing necessary cell-cell and cell-ECM interactions, cancer cells can maintain better their phenotype in 3D condition. The sheep liver extracellular matrix (LEM) already produced in our lab (45). Briefly, sheep liver was frozen and chopped into small pieces, and subjected to mechanical agitation 2.5 hours, in distilled water. The slices were then stirred in 1% sodium dodecyl

sulfate (SDS, Sigma, L3771, St. Louis, MO) at 4°C for 36 hours. Finally, decellularized pieces were stirred in deionized water at 4°C for 12 hours to remove the detergents and cellular fragments. To generate HCC-LEM, 1.5×10^5 Huh7 or HepG2 cells were seeded on the scaffold derived from LEM-Hydrogel. Then, both 3D constructs were cultured for 10 days.

Cell proliferation assay. To find 50% inhibitory activity (IA50s), total number of 2×10^4 cells/well were seeded in 96-well plates. At 75% – 80% confluency, cells were treated with 73 MBq of ^{188} Rhenium Perrhenate ($^{188}ReO_4$) (PARS ISOTOPE Company, Iran). After treatment with $^{188}ReO_4$ at different time points (18, 24, and 48 hours), 10 µL of ORANGU solution (Cell Guidance Systems; OR01-500) were added to each well. The plate incubated at 37°C for 2 hours. The absorbance values measured at 450 nm using a Stat Fax microplate reader (Awareness Technology, Inc., Palm City, FL). According to the kit data sheet, cell proliferation is proportional to optical density (OD).

Viability assay. Cells cultured in 2D condition and exposed to IA50 dose of $^{188}ReO_4$ at three time points, 18, 24, and 48 hours, harvested and suspended in PBS and evaluated by LIVE/DEAD® Viability/Cytotoxicity Kit (Invitrogen, L3224). The nuclei were counterstained with DAPI, and the viability assessment was visualized by green (live) or red (dead) fluorescence labelled cells using a fluorescence microscope (Olympus IX71, Tokyo, Japan).

Cell cycle analysis. Equal numbers of cells were dissociated using trypsin/EDTA (0.25%, Gibco; 25200056). Cells were fixed in 500 µL of 70% EtOH overnight at − 20°C. Fixed cells were washed and resuspended in FxCycle PI/RNase Staining Solution (ThermoFisher) at a concentration of 10^6 cells/ml and incubated at RT in a dark place 20 minutes before flow cytometry analysis (FACSCalibur, BD). The data were analyzed using FlowJo 10.6.2.

Apoptosis assessment with flow cytometric analysis. In 2D culture system, in order to determine the apoptosis rate in control and treatment groups after 18, 24, and 48 hours post exposure to IA50 dose, three replicates of $1x10^5$ Huh7 or HepG2 cells were incubated with fluorescein isothiocyanate (FITC)conjugated Annexin V and propidium iodide (556547, Annexin VFITC apoptosis detection kit, BD Pharmingen; BD Biosciences) on ice for 30 min. The cells were washed three times with PBS. Then, 400 µl binding buffer was added to the cells. Additionally, the cell suspension was analyzed by FACSCalibur. The data were analyzed using BD CellQuest™ Pro software (version 5.2.1; BD Biosciences) and the percentage of apoptotic cells per group were calculated.

Quantitative reverse transcriptase–polymerase chain reaction (qPCR). To evaluate of apoptosis and radio resistance signaling pathway in Huh7 /HepG2 cells treated with IA50s at the transcriptional level, we performed qRT-PCR for *p53*, *BAX*, *PTEN*, and *PI3K* genes. RNA extractions were performed using TRIzol (Invitrogen®), and then cDNA synthesized using PrimeScript™ Reverse Transcriptase Kit (Takara Bio, Inc., Kusatsu-Shi, Japan) according to the instructions from the manufacturer. Quantitative RT-PCR reactions were performed by a real-time PCR system (Applied Biosystems StepOne instrument, Foster City, CA) using SYBR Green Master Mix (Takara Bio, Inc., SYBR Premix) and the results analyzed by StepOne

software (Applied Biosystems; version 2.1). For each group, the samples were collected from three independent biological replicates. Finally, the expression levels of each target genes were normalized to *GAPDH.* Analysis was performed by the comparative CT Method $2^{-\Delta\Delta ct}$.

Histological and Immunofluorescence assessments. At the selected time points post-exposure from the both 3D constructs, the samples were harvested, fixed by 4% formaldehyde for overnight, and embedded in paraffin blocks. Then, 5-µm sections were prepared. To scrutinize the microstructure of the samples, H&E staining performed. In addition, to evaluate the expression of apoptosis related proteins, radio resistance and proliferation related proteins in both 3D constructs, immunostaining was performed to detect p53, BAX, P-AKT, and Ki67. The sections were incubated with primary antibodies overnight including mouse monoclonal antibody p53 (Santa Cruz, sc-126), BAX (Santa Cruz, sc-7480), rabbit polyclonal antibody P-AKT (sc-135650) and rabbit monoclonal antibody Ki67 (Cell Signaling Technology; #9129) at 4°C. Then, the sections were incubated with secondary antibody for 1 hour at 37°C. The nuclei were counterstained with DAPI, and the slides were analyzed under a fluorescent microscope (Olympus BX51).

Western blot. The 2D treated and control **c**ells were lysed in 1**X** RIPA buffer (Sigma-Aldrich) supplemented with Halt™ protease and phosphatase inhibitor cocktail (ThermoFisher Scientific). The protein concentration was determined by Bradford method. Equal concentration of protein extract was subjected to 12% SDS-PAGE and transferred to poly vinylidene fluoride (PVDF) membrane. Blots were labelled with the primary antibodies, p53 (1:500, Santa Cruz, sc-126), BAX (1:500, Santa Cruz, sc-7480), and P-AKT (1/500, Santa Cruz, sc-135650). B-actin was used as control. The day after, HRP-conjugated secondary antibody (1:5000, Sigma-Aldrich) was added to the blot for 3 hours at RT. Protein expression was detected using ECL western blotting detection reagent (Bio-Rad, Hercules, CA, USA) and membranes were imaged by ImageQuant LAS 4000 mini, GE Healthcare.

HCC mouse model. To evaluate tumorigenicity of cells, different numbers of Huh7 cells (3×10^6, 5×10^6, 7×10^6, and 10×10^6) subcutaneously injected to four anatomical sites in nude mice. When the tumors reached a visible size, tumors removed and their dimensions measured (Figure. Supplemnetary.1).

Tumor formation assay. To assess whether $^{188}ReO_4$ treated cells could form any tumor, Huh7 cells exposed to 37 MBq for 24 hours. The total number of 5×10^6 cells injected percutaneously to the flank of nude mice. As a control group, the same number (5×10^6) of untreated Huh7 cells injected percutaneously to the flank of another nude mouse. After 14 days, animals sacrificed for further assessments (Figure. Supplemnetary.1A).

Statistical analysis. All statistical analyses were performed using GraphPad-Prism, version 6. Data were presented as mean ± standard deviation (SD). In order to make statistical analysis between the treated and the control groups, the Kolmogorov-Smirnov normality tests were performed. These tests applied to find out which statistical test should be used to analyze the differences between the groups. Measurements were carried out using one-way repeated measures analysis of variance (ANOVA) and we

choose the LSD method for post Hoc multiple comparisons. The *p values* of less than 0.05 were considered as statistically significant.

Results

$^{188}ReO_4$ treatment reduced proliferation rate and viability in 2D cultured liver cancer cells

We performed a Live/dead staining test to determine changes in cell viability after exposure. As shown in Fig. 1A and D, the radionuclide exposure changed cell proliferation rate and viability. There was a difference in dead cell percentage at various radionuclide activities and different time points in two cell lines. The highest number of dead cell percentage was 69.19% treated with 55MBq of $^{188}ReO_4$ and 44.1% treated with 73MBq of $^{188}ReO_4$ at 48 h after exposure for Huh7 and HepG2 cells, respectively. The impact of $^{188}ReO_4$ exposure on human dermal fibroblasts (HDF) as a normal cell was evaluated. The viability of HDF cells did not changed after incubation with $^{188}ReO_4$. As shown in Fig. 1B, and E, $^{188}ReO_4$ induced cytotoxicity in human liver cancer cell lines in a dose-dependent manner. Notably, two hepatoma cell lines exhibited different sensitivities to $^{188}ReO_4$. While the IA50 value of $^{188}ReO_4$ for Huh7 was 37 MBq at 24 h post exposure, the IA50 value for HepG2 was 55 MBq at 48 h post exposure. The results indicated that the Huh7 cells was more sensitive to $^{188}ReO_4$ exposure. Finally, 37 MBq and 55 MBq were chosen as IA50 dose for Huh7 and HepG2 cells respectively to perform further analysis.

$^{188}ReO_4$ induced G2/M arrest in Huh7 cancer cells.

The effect of $^{188}ReO_4$ exposure with IA50 doses on the cell cycle progression assessed for both cell lines after 18, 24, and 48 h. FACS analysis showed that 37 MBq exposure resulted in significant G2/M arrest of Huh7 cells, while for HepG2, 55MBq exposure did not make significant changes in cell cycle phases (Fig. 2A and B). We also observed significant arrest after 24 h, however, after 48 h of exposure, cells had either entered sub-G1 phase (cell death) or reverted to normal cell cycle in Huh7. Interestingly, G2/M arrest did not observe in HepG2 cells. Cell cycle analysis after exposure to 55 MBq in HepG2 cells showed reduction of cells in S phase with a concomitant increase in the G2 and G1 phase of the cell cycle, with minor impact on the sub-G1 phase at 18 and 48 hours post exposure respectively.

Furthermore, to evaluate the effects of $^{188}ReO_4$ treatment on colony formation capability, Huh7 and HepG2 cells that treated with 37 MBq and 55 MBq seeded in culture plates. Data showed almost three folds less colonies than untreated control cells (Fig. 2C and D).

$^{188}ReO_4$ induced apoptosis in hepatic cancer cells

For further investigation, the apoptosis induction after exposure to $^{188}ReO_4$ measured using Annexin V-APC/7-AAD (Fig. 3A, B, C, and D). Statistically significant ($p < 0.05$) increase in the number of apoptotic

cells observed after treatment in Huh7 cells at 24 and 48 h (Fig. 3C). Apoptotic cells increased significantly in HepG2 cells after 18 and 48 h post exposure (Fig. 3D).

The mRNA expression of *p53* and *Bax* analyzed after treatment with $^{188}ReO_4$ in Huh7 and HepG2 cells. Compared to control group, Huh7 cells displayed increased *p53* relative mRNA expression after 24 h post exposure, while in HepG2 cells there was no significant difference in mRNA expression (Fig. 3E and G). The qRT-PCR analysis revealed that mRNA level of *Bax* was significantly higher in Huh7 cells after 24 and 48 h post exposure with 37 MBq of $^{188}ReO_4$ (Fig. 3F). The *Bax* expression after 18 and 24 h post exposure with 55 MBq of $^{188}ReO_4$ showed significant increase in HepG2 cells (Fig. 3H).

Western blot assay data showed, significant increase of p53 and BAX proteins in Huh7 cells, while there are no remarkable differences in p53 and BAX expression in HepG2 cells after exposure to $^{188}ReO_4$ (Fig. 3I).

$^{188}ReO_4$ exposure reduced cell viability in both cell lines in 3D LEM constructs

Orangu® assay performed on the Huh7-LEM and HepG2-LEM after $^{188}ReO_4$ treatment with 37, 55, and 73 MBq to determine total cell viability and effective activity dose. Samples collected after 18, 24, and 48 h following the exposure. Cell viability in both 3D constructs after exposure declined up to 50% (IA50) by using 55 MBq of radionuclide from 18 to 48 h (Fig. 4B and C).

Ki-67 specific staining visualized in Fig. 4D and F. The proliferative cells presented bright red nucleus after immunostaining. Following 48 h exposure to 55 MBq, Ki-67 positive cells in both 3D constructs decreased (Fig. 4E).

$^{188}ReO_4$ induced apoptosis in cells cultured on both 3D constructs

Radionuclide exposure affects the *p53* and *Bax* mRNA expression levels in both 3D constructs (Fig. 4G). Following 18, 24, and 48 h exposure to 55 MBq of radionuclide, *p53* mRNA levels in Huh7-LEM showed significant difference at 18 and 24 h compared to untreated control group; while there are no tangible differences in *p53* gene expression after exposure in HepG2-LEM group. To show whether 55 MBq of exposure by $^{188}ReO_4$ induce apoptosis in both 3D constructs, the mRNA abundance of a pro-apoptotic gene *Bax* quantified. Outcomes showed significant differences in *Bax* gene expression at 24 and 48 h after exposure in Huh7-LEM. However, there was a significant increase in *Bax* mRNA expression only 48 h after exposure in HepG2-LEM (Fig. 4G).

To assess whether $^{188}ReO_4$ exposure promotes p53 and Bax protein expression in both 3D constructs treated with 55 MBq of radionuclide, immunofluorescence staining performed. The IF images indicated that $^{188}ReO_4$ treatment resulted in upregulation of p53 protein in Huh7-LEM compare to the control group (Fig. 4H, L), whereas there were no significant changes in p53 in HepG2-LEM (Fig. 4J, L). There were increased Bax protein post exposure in both 3D constructs compared to their control groups (Fig. 4L).

These findings suggest that $^{188}ReO_4$ induced Bax protein upregulation and facilitated the pro-apoptotic function of Bax in both 3D constructs.

^{188} ReO $_4$ overcome radio-resistance in 2D but not in 3D

The qRT-PCR performed to determine whether PTEN, and PI3K contribute to radio- resistance after exposure to $^{188}ReO_4$ in 2D and 3D. We analyzed mRNA expression in 2D samples from Huh7 and HepG2 cells. *PTEN* and *PI3K* transcript levels were consistent after 18, 24, and 48 h exposure with 37 and 55 MBq in Huh7 and HepG2 cells, respectively (Fig. 5A). To determine the effects of IA50 dose exposure on P-AKT in 2D condition, we performed western blot (Fig. 5B). Our data revealed that $^{188}ReO_4$ exposure induced significant reduction of P-AKT at protein level compare to control groups in both cell lines (Fig. 5B).

To quantify the expression of *PTEN*, and *PI3K* in both 3D constructs we first analysed the expression levels of mRNAs post exposure of 55 MBq to $^{188}ReO_4$ at 18, 24, and 48 h. The qRT-PCR data for *PTEN* mRNA expression did not show any significant difference in 3D culture of Huh7-LEM; while in HepG2-LEM, there was a significant increase of *PTEN* gene expression at 24 h post exposure. The qRT-PCR data of *PI3K* expression for treated Huh7-LEM and HepG2-LEM were similar at 24 and 48 h post exposure. The up-regulation of *PI3K* observed in both 3D constructs after exposure (Fig. 5C and D).

Both 3D cultured constructs were treated with $^{188}ReO_4$, 55 MBq. The P-AKT protein were evaluated using IF staining. The P-AKT expression was up-regulated after exposure with effective dose of radionuclide in Huh7-LEM construct, howerver no difference observed in HepG2-LEM constract (Fig. 5E and F).

^{188} ReO $_4$ treated cells did not initiate and develop tumor in animal study

The total number of 5×10^6 $^{188}ReO_4$ treated Huh7 cells and non-treated Huh7 cells injected percutaneously to the flank of nude mice. Treated cells exposed to 37 MBq for 24 hours. After 14 days, animals sacrificed for further assessments (Figure. Supplemnetary.1B). The non-treated cells developed a visible and palpable mass in the right flank of the nude mouse. The nude mouse received treated Huh7 cells did not have any tumor in the sight of injection.

Discussion

Rhenium-188 is produced by $^{188}W/^{188}Re$ generator in a convenient and inexpensive way in the hospitals (46). Different Derivatives of $^{188}ReO_4$ transarterialy injected to HCC tumores and are under development as a targeting radionuclide for therapeutic purposes (12, 13, 46, 47).

In past decades, cancer cell lines have played important role in revealing molecular mechanisms in initiation and developing new drugs (48). The rationale for using cancer cell lines as an experimental model is that cancer cell lines retain the hallmarks of primary cancer cells (49). Although two-dimensional

(2D) cell culture systems are efficient and reliable, the lack of appropriate cell-cell and cell-ECM contact is typically observed compared to the *in vivo*. It has been demonstrated that three-dimensional (3D) organotypic human cancer cell models are suitable alternatives to mimic tumor microenvirounment (19–21).

The present study discussed ablative effect of $^{188}ReO_4$ on the hepatic cancer cell lines, in 2D and 3D culture systems, and mouse model. Data showed that dose and time of exposure to $^{188}ReO_4$ affected the viability rate. In addition, IA50 doses and dead cell percentages were different between 2D and 3D cultured cells. The IA50 value for Huh7 cells was 37 MBq at 18, 24, and 48 h after exposure to $^{188}ReO_4$ whereas, in HepG2 cells, it was 55 MBq at 48 h post-exposure. The above results associated with the flow cytometric results for the cell cycle phases in both lines. Flow analysis data showed a significant dose and time dependant reduction in HepG2 cells for the S phase, while the G2/M phase increased in Huh7 cells. Other studies demonstrated that the rhenium components induced cell cycle arrest at the G2/M phase by inhibiting the phosphorylation of Aurora-A kinase (50, 51). In our study, cell cycle analysis showed a dose-dependent block in G2/M phase that was in line with the results of Gilbertz and colleages (52). In addition, the percentage of emerged colonies was decreased significantly in both Huh7 and HepG2 cells after treatment by effective doses of $^{188}ReO_4$.

The viability percentage was higher than 60% for HDF as normal cells. Live and dead staining assay for Huh7 and HepG2, suggested that $^{188}ReO_4$ treatment was effective on the mortality rate of both cells, whereas the exposure on HDF cells did not result in the same percentage of dead cells. Information on the toxicity of radionuclides on the normal tissues is more limited than that from external beam radiation and appears to be more variable (53). Intrestingly, we showed that the effective doses of $^{188}ReO_4$ for HCC cell lines were well tolerated in fibroblasts (HDF). The tolerance of normal tissues after radiation is higher but more variable, however. this variability is more attributed to the differences in dosimetry method and to the heterogeneous distribution of the radionuclides (53). Heterogeneity of dose absorbtion at the cellular level remained a concern for radionuclides (54). The Wellcome Trust Case Control Consortium at www.wtccc.org.uk continues to study genetic differences in a large population of healthy and diseased. Their data could enable researchers to perform metaanalysis to various models to reach the best estimate of tolerance in normal and cancer cells (53).

Limitations of 2D culture were always apparent, including the lack of tissue-specific architecture and altered or absent cell–cell and cell–ECM interactions that could contribute to development or maintenance of the tumor (55). In 3D culture, the calculated effective dose for Huh7-LEM and HepG2-LEM was 55 MBq at 18, 24, and 48 h after exposure. IA50 for Huh7-LEM increased, compared to 2D culture, while the effective dose was the same for HepG2 cells in 2D and 3D. Previous studies showed that tumor cells in scaffolds, received less exposure to therapeutic agents since diffusion of therapeutic agents into the tumor mass is limited (56). Various studies demonstrated that enrichment of microenvironment with ECM components enhanced the viabilities of normal and tumor cells (57, 58). The mean percentage of proliferative cells in 3D treated groups compared to the control were 6.5% and 7.9%

for Huh7 and HepG2, respectively. In HCC-LEMs, decrease in proliferation rate indicated that $^{188}ReO_4$ penetrated well in the 3D structures and affected cancers cells.

Overall, cell proliferation was altered in association with the radiation dose and exposure time. Both HUH7 and Hep G2 Cells treated with less than 37 MBq or 55 MBq as their IA50 showed no significant growth inhibition afetr 48 h.

Evidences to proof apoptosis induction after $^{188}ReO_4$ exposure obtained from the results of the flow cytometric, qPCR, and western blot experiments. The Annexin/PI flow cytometeric results showed that the DNA damage induced by 37 MBq of $^{188}ReO_4$ increased apoptosis induction significantly at 24 and 48 h post-exposure in Huh7. Furthermore, we reported apoptosis induction after 55 MBq exposure at 18 and 48 h in HepG2.

Radiotherapy is one of the most effective modalities for cancer treatment and P53 is a key molecule involved in cellular response to ionizing radiation (36, 59, 60). Given the importance of P53 expression in the development of response to treatment in many types of tumors, and in order to determine the effectiveness of radiotherapy in different HCC cell lines, we evaluated the P53 expression. HuH7 and HepG2 have basal P53 protein expression (61, 62), although *p53* mRNA expression differs significantly across the two lines. $^{188}ReO_4$ induced *p53* mRNA expression in Huh7 cells after 24 h, whereas there was not an increased expression of *p53* in HepG2 cells. Immunoblotting results showed increased P53 protein expression in Huh7 cells after exposure to 37 MBq with $^{188}ReO_4$, whereas there was not any significant changes in P53 protein expression in HepG2 cells after exposure to 55 MBq. Apoptosis of tumour cells by induction of Bax, P53 and caspase mediated cleavage of p21 is an important radiation-induced cell death mechanisms (63). In order to confirm if P53 protein triggered the apoptosis after irradiation in HepG2 and HuH7 cell lines, *BAX* mRNA and protein expressions were evaluated. It was verified that the *BAX* mRNA up regulated at 24 and 48 h post exposure in Huh7 cells and 24 h after exposure in HepG2 cells. The Bax protein expression was significant in Huh7 cells, whereas there was unchanged protein expression of BAX in HepG2 cells. Scince the protein expression of BAX in HepG2 cells was not absorved, apoptosis can be derived from the direct effect of O_2 free radicals (64). Reactive oxygen species like H_2O_2 or OH, can cause Ca^{2+} release from mitochondria, provoking various pro-apoptotic consequences (65, 66).

The qRT-PCR data showed signifcant differences in *p53* mRNA expression in treated Huh7-LEM with 55 MBq after 48 h compared to control group, while, in HepG2-LEM, there are not any notable changes in *p53* mRNA expression. The immunohistofluorescence analysis of p53 showed apoptosis induction after $^{188}ReO_4$ treatment in Huh7-LEM, wherease the same result not seen in HepG2-LEM. The *Bax* mRNA expressions in $^{188}ReO_4$ treated HCC-LEM were upregulated at 24 and 48 h post treatment for Huh7-LEM and 48 h for HepG2-LEM. These findings demonstrated that $^{188}ReO_4$ can induce cell apoptosis and inhibit cell proliferation in HCC cells, providing evidence for the internal application.

The mRNA and protein expression of the p53 was not changed in cells cultured on 3D LEM compared to 2D cultured cells. This trend was same for *Bax* mRNA and protein expression in 2D culture for Huh7 and Huh7-LEM. The *p53* mRNA and protein expression in both 2D and 3D had the same patern, whereas for Bax we showed reverse results of mRNA and protein expression in 2D compared to 3D. In case of *Bax* mRNA and protein expression in 2D and 3D, the microenvironment conditions produced in our LEM 3D culture could induce significant changes in cellular behavior as compared to conventional 2D culture, consistent with many studies on microenvironment-mediated factors (56, 67–71). In this study, we showed that $^{188}ReO_4$ induced apoptosis and cell cycle arrest in HCC cells, in a dose and time dependent manner in both 2D and 3D culture.

The PI3K/AKT signaling pathway has been extensively studied and demonstrated to be essential for radiotherapy resistance in various cancer types (72–74). DNA-dependent protein kinase (DNA-PK) is a protein complex, which is essential for the DSBs repair (75). The phosphorylation of DNA-PKcs (T2609) is related to the DSB repair and radiosensitivity of cells (75). It has been reported that the PI3K/Akt pathway was involved in the regulation of DNA-PKcs (76). In the present study, it was observed that mRNA expression of *PTEN* as PI3K/AKT inhibitor and PI3K has not changed after exposure to IA50 dose of $^{188}ReO_4$ in 2D culture systems. Western blot data showed AKT-P protein decreased in both Huh7 and HepG2 cells significantly after exposure. We did not observed any considerable changes in *PTEN* mRNA expression in HCC-LEMs, wherease *PI3K* mRNA expression increased 24 and 48 h post exposure in Huh7-LEM, and 18,24, and 48 hours after treatmend in HepG2-LEM. Immonublotting results showed a significant increase in AKT-P protein expression in treated Huh7-LEM, wherease there was not any notable changes in protein expression of AKT-P in HepG2-LEM after exposure. Previous studies suggested that the scaffold increased the resistance to treatment in HCC 3D culture systems (77). There are several reports that decellularized scaffolds are useful in drug discovery (78). The natural ECM enables HCC cells to sustain their original capabilities in drug metabolism and proliferation (78). Therefore, HCC cells cultured in decellularized 3D scaffolds can provide better platform for drug toxicity than conventional 2D culture systems (78, 79).

Conclusions

In this study, we developed 2D, 3D, and *in vivo* model of HCC to evaluate the therapeutic effects of $^{188}ReO_4$. Although, there are differences in IA50s of $^{188}ReO_4$ in various models for each cancerous cell, our study indicated that treatment with $^{188}ReO_4$ had remarkable impact on prolifferation inhibition in all the models. It seem that different responses to the irradiation depends on initial differences of the cell's heterogenecity and genetic discrepancy in 2D models, microinviroment variations in 3D models, and *in vivo* condition in animal models. Generally, cell viability values were time and dose depandent in all models. We have shown that $^{188}ReO_4$ radiation induced the expression of genes that are involved in apostosis. Our expression analysis results were consistent with western bloting and immunohistochemistry analysis of *bax*, which showed apoptosis in all 2D and 3D HCC models wherease the data for *p53* in mRNA and protein expression in all in vitro models were different. Overall, these

findings demonstrated that $^{188}ReO_4$ can induce cell apoptosis and inhibit proliferation, providing adequate evidences of its potential for the internal radiotherapy of HCC.

In this study we also highlighted the role of PI3K-Akt signaling pathway in inducing resistance to irradiation. Interestingly, we observed that there are differences in p-AKT protein expression in 2D and 3D models. We suggest that the ECM as the cells scafold can have a remarkable role in radio-resistance. In adition, we could show that treatment of HCC cells with $^{188}ReO_4$ displayed significant anti-tumor activity *in-vivo* and caused regression of established cancer and tumor models in nude mice. More studies needed to find other aspects of the impact of $^{188}ReO_4$ in HCC treatment. This preliminary study provided a preliminary roadmap for finding a comprehensive data for studying radiobiology of therapeutical radionuclides in HCC.

Abbreviations

2D
two-dimensional
^{188}Re
Rhenium-188
ECM
extracellular matrix
FBS
fetal bovine serum
FITC
fluorescein isothiocyanate
HBV
hepatitis B virus
HCC
hepatocellular carcinoma
HCV
hepatitis C virus
HDF
human dermal fibroblast
HGDMEM
high-glucose Dulbecco’s modified Eagle’s medium
IA50
50% inhibitory activity
IF
immunofluorescence
LEM
liver extracellular matrix

TACE
transarterial chemoembolization

Declarations

Ethics approval and consent to participate: The animal experiments were approved by the Local Ethical Committee of the Royan institute. The ID code number is IR.ACECR.ROYAN.REC.1397.052.

Consent for publication: Not applicable.

Availability of data and material: The data supporting the findings are available and can be provided upon request.

Funding: This study was financially supported by the “National Cancer Control Charity Foundation, registration number 41476, Tehran, IRAN". AS, VK, and PT were supported by the Ministry of Science and Higher Education of the Russian Federation within the framework of state support for the creation and development of World-Class Research Centers «Digital biodesign and personalized healthcare» (agreement № 075-15-2020-926).

Authors' contributions: S.A. performed the experiments and data collection and drafting the manuscript. A.P., N.G., P.T., and M.H contributed in the development of concept, study design and critical reviewing the manuscript. B.A.K., M.R.D., and M.M. contributed in study design and prepration of radionuclide, calculations for exposure, data analysis and reviewing the manuscript. S.S., M.A., V.K., S.M.N., and A.S. contributed in study design, data collection and data analysis and drafting the results. M.V. developed the concept, contributed in data analysis, critical reviewing and approval of the manuscript and financial supporting the project.

Competing Interests: The authors declare no conflict of interest.

References

1. Bray F, Ferlay J, Soerjomataram I, Siegel RL, Torre LA, Jemal AJCacjfc. Global cancer statistics 2018: GLOBOCAN estimates of incidence and mortality worldwide for 36 cancers in 185 countries. 2018;68(6):394–424.
2. El-Serag HBJTLB. Pathobiology. Epidemiology of hepatocellular carcinoma. 2020:758–72.
3. Lasfar A. Introductory Chapter: Liver Cancer, Risk Factors and Current Therapies. Liver Cancer: IntechOpen; 2018.
4. Ryder SDJG. Guidelines for the diagnosis and treatment of hepatocellular carcinoma (HCC) in adults. 2003;52(suppl 3):iii1-iii8.
5. Zhou J, Sun H-C, Wang Z, Cong W-M, Wang J-H, Zeng M-S, et al Guidelines for diagnosis and treatment of primary liver cancer in China (2017 Edition). 2018;7(3):235 – 60.

6. Hernaez R, El-Serag HBJAJoG. How we approach it: treatment options for hepatocellular carcinoma. 2018;113(6):791–4.
7. Lau WY, Teoh YL, Win KM, Lee R-C, De Villa VH, Kim YHJ, et al. Current role of selective internal radiation with yttrium-90 in liver tumors. 2016;12(9):1193–204.
8. Edeline J, Gilabert M, Garin E, Boucher E, Raoul J-LJLC. Yttrium-90 microsphere radioembolization for hepatocellular carcinoma. 2015;4(1):16–25.
9. Xu J, Shen ZY, Chen XG, Zhang Q, Bian HJ, Zhu P, et al. A randomized controlled trial of Licartin for preventing hepatoma recurrence after liver transplantation. 2007;45(2):269–76.
10. Raoul J-L, Guyader D, Bretagne J-F, Duvauferrier R, Bourguet P, Bekhechi D, et al. Randomized controlled trial for hepatocellular carcinoma with portal vein thrombosis: intra-arterial iodine-131-iodized oil versus medical support. 1994;35(11):1782–7.
11. Uccelli L, Martini P, Pasquali M, Boschi AJBri. Monoclonal antibodies radiolabeling with Rhenium-188 for radioimmunotherapy. 2017;2017.
12. Gallicchio R, Nardelli A, Mainenti P, Nappi A, Capacchione D, Simeon V, et al. Therapeutic strategies in HCC: radiation modalities. 2016;2016.
13. Seelam SR, Banka VK, Lee Y-S, Jeong JMJJoR, Probes M. 188 Re Labeled liver therapeutic drugs for hepatic carcinoma (HCC). 2019;5(1):26–35.
14. Yamada KM, Cukierman EJC. Modeling tissue morphogenesis and cancer in 3D. 2007;130(4):601–10.
15. Hirschhaeuser F, Menne H, Dittfeld C, West J, Mueller-Klieser W. Kunz-Schughart LAJJob. Multicellular tumor spheroids: an underestimated tool is catching up again. 2010;148(1):3–15.
16. Rimann M, Graf-Hausner, UJCoib. Synthetic 3D multicellular systems for drug development. 2012;23(5):803–9.
17. Lovitt CJ, Shelper TB, Avery VMJB. Advanced cell culture techniques for cancer drug discovery. 2014;3(2):345–67.
18. Weigelt B, Ghajar CM, Bissell MJJAddr. The need for complex 3D culture models to unravel novel pathways and identify accurate biomarkers in breast cancer. 2014;69:42–51.
19. Debnath J, Brugge JSJNRC. Modelling glandular epithelial cancers in three-dimensional cultures. 2005;5(9):675–88.
20. Ridky TW, Chow JM, Wong DJ. Khavari PAJNm. Invasive three-dimensional organotypic neoplasia from multiple normal human epithelia. 2010;16(12):1450–5.
21. Xia L, Sakban RB, Qu Y, Hong X, Zhang W, Nugraha B, et al. Tethered spheroids as an in vitro hepatocyte model for drug safety screening. 2012;33(7):2165–76.
22. Hamilton GA, Westmoreland C, George EJIVC, Biology-Animal D. Effects of medium composition on the morphology and function of rat hepatocytes cultured as spheroids and monolayers. 2001;37(10):656.

23. Abu-Absi SF, Friend JR, Hansen LK, Hu W-SJEcr. Structural polarity and functional bile canaliculi in rat hepatocyte spheroids. 2002;274(1):56–67.
24. Yamashita T, Ji J, Budhu A, Forgues M, Yang W, Wang HY, et al. EpCAM-positive hepatocellular carcinoma cells are tumor-initiating cells with stem/progenitor cell features. 2009;136(3):1012–24. e4.
25. Kumar C, Sharma R, Vats K, Mallia MB, Das T, Sarma H, et al. Comparison of the efficacy of 177 Lu-EDTMP, 177 Lu-DOTMP and 188 Re-HEDP towards bone osteosarcoma: an in vitro study. 2019;319(1):51–9.
26. Zhang J, Su G, Lin Y, Meng W, Lai JKL, Qiao L, et al. Targeting Cyclin-dependent Kinases in Gastrointestinal Cancer Therapy. 2019;27(146):27–36.
27. Liu R, Zhao T, Swat MH, Reynoso FJ, Higley KAJIjorb. Development of computational model for cell dose and DNA damage quantification of multicellular system. 2019;95(11):1484–97.
28. Roobol SJ, Hartjes TA, Slotman JA, de Kruijff RM, Torrelo G, Abraham TE, et al. Uptake subcellular distribution of radiolabeled polymersomes for radiotherapy. 2020;4(1):14.
29. Falzone N, Ackerman NL, de la Fuente Rosales L, Bernal MA, Liu X, Peeters SG, et al. Dosimetric evaluation of radionuclides for VCAM-1-targeted radionuclide therapy of early brain metastases. 2018;8(1):292.
30. Terry SY, Nonnekens J, Aerts A, Baatout S, de Jong M, Cornelissen B, et al. Call to arms: need for radiobiology in molecular radionuclide therapy. 2019;46(8):1588–90.
31. Mirzaie-Joniani H, Eriksson D, Sheikholvaezin A, Johansson A, Löfroth PO, Johansson L, et al. Apoptosis induced by low-dose and low-dose-rate radiation. 2002;94(S4):1210–4.
32. Wendt J, von Haefen C, Hemmati P, Belka C, Dörken B, Daniel PTJO. TRAIL sensitizes for ionizing irradiation-induced apoptosis through an entirely Bax-dependent mitochondrial cell death pathway. 2005;24(25):4052–64.
33. Zhang J, Hong C, Zhu SJJoRR, Processing R. The characteristics and mechanism of apoptosis in K 562 cells induced by radionuclides strontium-89. 2003;21(1):77–80.
34. Lee J, Yang W, Lee M-G, Ryu Y, Park J, Shin K-H, et al. Effective local control of malignant melanoma by intratumoural injection of a beta-emitting radionuclide. 2002;29(2):221–30.
35. Gomes AR, Abrantes AM, Brito AF, Laranjo M, Casalta-Lopes JE, Gonçalves AC, et al. Influence of P53 on the radiotherapy response of hepatocellular carcinoma. 2015;21(3):257.
36. Cuddihy AR, Bristow RGJC, Reviews M. The p53 protein family and radiation sensitivity: Yes or no? 2004;23(3–4):237–57.
37. Ma Z-H, Yang Y, Zou L, Luo K-YJJoE, Research CC. 125I seed irradiation induces up-regulation of the genes associated with apoptosis and cell cycle arrest and inhibits growth of gastric cancer xenografts. 2012;31(1):61.
38. Vinci M, Gowan S, Boxall F, Patterson L, Zimmermann M, Lomas C, et al. Advances in establishment and analysis of three-dimensional tumor spheroid-based functional assays for target validation and

drug evaluation. 2012;10(1):29.
39. Leong DT, Ng, KWJAddr. Probing the relevance of 3D cancer models in nanomedicine research. 2014;79:95–106.
40. Hutmacher DW, Loessner D, Rizzi S, Kaplan DL, Mooney DJ. Clements JAJTib. Can tissue engineering concepts advance tumor biology research? 2010;28(3):125–33.
41. Badylak SF, Freytes DO. Gilbert TWJAb. Extracellular matrix as a biological scaffold material: structure and function. 2009;5(1):1–13.
42. Saldin LT, Cramer MC, Velankar SS, White LJ, Badylak SFJAb. Extracellular matrix hydrogels from decellularized tissues: structure and function. 2017;49:1–15.
43. Dunne LW, Huang Z, Meng W, Fan X, Zhang N, Zhang Q, et al. Human decellularized adipose tissue scaffold as a model for breast cancer cell growth and drug treatments. 2014;35(18):4940–9.
44. Nietzer S, Baur F, Sieber S, Hansmann J, Schwarz T, Stoffer C, et al. Mimicking metastases including tumor stroma: a new technique to generate a three-dimensional colorectal cancer model based on a biological decellularized intestinal scaffold. 2016;22(7):621–35.
45. Saheli M, Farzaneh Z, Taheri P, Dorraj M, Baharvand H, Vosough M, et al. Generation of Transplantable Three-Dimensional Hepatic-Patch to Improve the Functionality of Hepatic Cells In Vitro and In Vivo. 2020;29(5):301–13.
46. Lepareur N, Lacœuille F, Bouvry C, Hindré F, Garcion E, Chérel M, et al. Rhenium-188 Labeled Radiopharmaceuticals: Current Clinical Applications in Oncology and Promising Perspectives. 2019;6(132).
47. Lepareur N, Garin EJIJNMR. Transarterial radionuclide therapy with 188Re-labelled lipiodol. 2017:79–91.
48. Sharma SV, Haber DA. Settleman JJNrc. Cell line-based platforms to evaluate the therapeutic efficacy of candidate anticancer agents. 2010;10(4):241–53.
49. Masters JRJNrMcb. Human cancer cell lines: fact fantasy. 2000;1(3):233–6.
50. Simpson P, Casari I, Paternoster S, Skelton B, Falasca M, Massi MJCAEJ. Defining the anti-cancer activity of tricarbonyl rhenium complexes: induction of G2/M cell cycle arrest and blockade of Aurora-A kinase phosphorylation. 2017.
51. Simpson PV, Falasca M, Massi MJCC. Properties and prospects for rhenium (i) tricarbonyl N-heterocyclic carbene complexes. 2018;54(88):12429–38.
52. GILBERTZ D. VAN BEUNINGEN AP RHEIN K-PJIjorb. Early changes in cell cycle kinetics after ionizing irradiation below 1. Gy. 1998;73(2):187–95.
53. Meredith R, Wessels B, Knox S, editors. Risks to normal tissues from radionuclide therapy. Seminars in nuclear medicine; 2008: Elsevier.
54. Neti PV, Howell RWJJoNM. Log normal distribution of cellular uptake of radioactivity: implications for biologic responses to radiopharmaceuticals. 2006;47(6):1049–58.

55. Kim JB, editor Three-dimensional tissue culture models in cancer biology. Seminars in cancer biology; 2005: Elsevier.
56. Minchinton AI, Tannock IFJNRC. Drug penetration in solid tumours. 2006;6(8):583–92.
57. Lee JS, Shin J, Park H-M, Kim Y-G, Kim B-G, Oh J-W, et al. Liver Extracellular Matrix Providing Dual Functions of Two-Dimensional Substrate Coating and Three-Dimensional Injectable Hydrogel Platform for Liver Tissue Engineering. Biomacromol. 2014;15(1):206–18.
58. Zhang Y, He Y, Bharadwaj S, Hammam N, Carnagey K, Myers R, et al. Tissue-specific extracellular matrix coatings for the promotion of cell proliferation and maintenance of cell phenotype. Biomaterials. 2009;30(23):4021–8.
59. Begg AC, Stewart FA, Vens CJNRC. Strategies to improve radiotherapy with targeted drugs. 2011;11(4):239–53.
60. Levine AJ, Oren MJNrc. The first 30 years of p53: growing ever more complex. 2009;9(10):749–58.
61. He M, Zhao M, Shen B, Prise K, Shao CJO. Radiation-induced intercellular signaling mediated by cytochrome-c via a p53-dependent pathway in hepatoma cells. 2011;30(16):1947–55.
62. Bressac B, Galvin KM, Liang TJ, Isselbacher KJ, Wands JR. Ozturk MJPotNAoS. Abnormal structure and expression of p53 gene in human hepatocellular carcinoma. 1990;87(5):1973–7.
63. Zhang Y, Fujita N, Tsuruo TJO. Caspase-mediated cleavage of p21 Waf1/Cip1 converts cancer cells from growth arrest to undergoing apoptosis. 1999;18(5):1131–8.
64. Maier P, Hartmann L, Wenz F, Herskind CJIjoms. Cellular pathways in response to ionizing radiation and their targetability for tumor radiosensitization. 2016;17(1):102.
65. Ogura A, Oowada S, Kon Y, Hirayama A, Yasui H, Meike S, et al. Redox regulation in radiation-induced cytochrome c release from mitochondria of human lung carcinoma A549 cells. 2009;277(1):64–71.
66. Richter C, Frei BJFRB. Medicine. Ca2 + release from mitochondria induced by prooxidants. 1988;4(6):365–75.
67. Spangenberg HC, Thimme R. Blum HEJNrG, hepatology. Targeted therapy for hepatocellular carcinoma. 2009;6(7):423.
68. Fischbach C, Chen R, Matsumoto T, Schmelzle T, Brugge JS, Polverini PJ, et al. Engineering tumors with 3D scaffolds. 2007;4(10):855–60.
69. Wu XZ, Chen D, Xie GRJMh. Extracellular matrix remodeling in hepatocellular carcinoma: effects of soil on seed? 2006;66(6):1115–20.
70. Meads MB, Gatenby RA, Dalton, WSJNrc. Environment-mediated drug resistance: a major contributor to minimal residual disease. 2009;9(9):665–74.
71. Sermeus A, Cosse J-P, Crespin M, Mainfroid V, de Longueville F, Ninane N, et al. Hypoxia induces protection against etoposide-induced apoptosis: molecular profiling of changes in gene expression and transcription factor activity. 2008;7(1):27.
72. Chang L, Graham PH, Ni J, Hao J, Bucci J, Cozzi PJ, et al. Targeting PI3K/Akt/mTOR signaling pathway in the treatment of prostate cancer radioresistance. 2015;96(3):507–17.

73. Heavey S, O'Byrne KJ, Gately KJCtr. Strategies for co-targeting the PI3K/AKT/mTOR pathway in NSCLC. 2014;40(3):445–56.
74. Bamodu OA, Chang H-L, Ong J-R, Lee W-H, Yeh C-T, Tsai J-TJC. Elevated PDK1 Expression Drives PI3K/AKT/MTOR Signaling Promotes Radiation-Resistant and Dedifferentiated Phenotype of Hepatocellular Carcinoma. 2020;9(3):746.
75. Burma S, Chen DJJDr. Role of DNA–PK in the cellular response to DNA double-strand breaks. 2004;3(8–9):909–18.
76. Toulany M, Kasten-Pisula U, Brammer I, Wang S, Chen J, Dittmann K, et al. Blockage of epidermal growth factor receptor-phosphatidylinositol 3-kinase-AKT signaling increases radiosensitivity of K-RAS mutated human tumor cells in vitro by affecting DNA repair. 2006;12(13):4119–26.
77. Leung M, Kievit FM, Florczyk SJ, Veiseh O, Wu J, Park JO, et al. Chitosan-alginate scaffold culture system for hepatocellular carcinoma increases malignancy and drug resistance. 2010;27(9):1939–48.
78. Hussein KH, Park KM, Ghim JH, Yang SR, Woo HMJJobmrpBab. Three dimensional culture of HepG2 liver cells on a rat decellularized liver matrix for pharmacological studies. 2016;104(2):263–73.
79. Mazza G, Rombouts K, Hall AR, Urbani L, Luong TV, Al-Akkad W, et al. Decellularized human liver as a natural 3D-scaffold for liver bioengineering and transplantation. 2015;5(1):1–15.

Figures

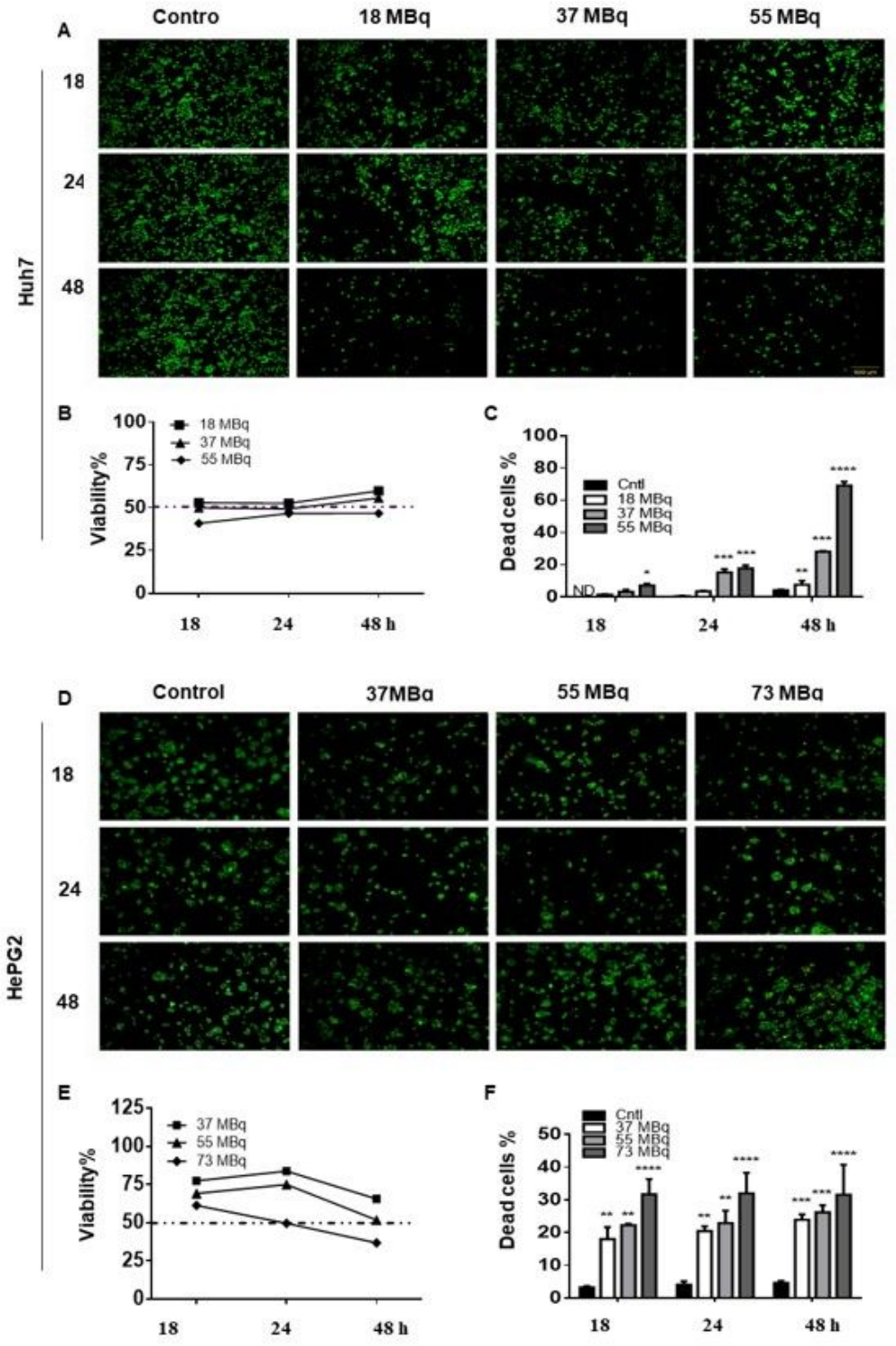

Figure 1

Cells viability assay and IA50 dose finding. A. Huh7 cells viability. Merged live and dead assay for control (untreated), 18, 37, and 55 MBq treated groups with 188ReO4 after 18, 24, and 48 h post exposure. B, C. Mean viable and dead cells in percent versus control for finding effective dose of 188ReO4 in Huh7 treated cells. Data presented as the mean ± SD, n = 3 (* P<0.05, ** P<0.001, *** P<0.0001) D. HepG2 cells viability. Merged live and dead assay for control (untreated), 37, 55, and 73 MBq treated groups with

188ReO4 after 18, 24 and 48 hours post exposure. E, F. Mean viable and dead cells in percent versus control for finding effective dose of 188ReO4 in HepG2 treated cells. Data presented as the mean ± SD, n = 3 (* P<0.05, ** P<0.001, *** P<0.0001)

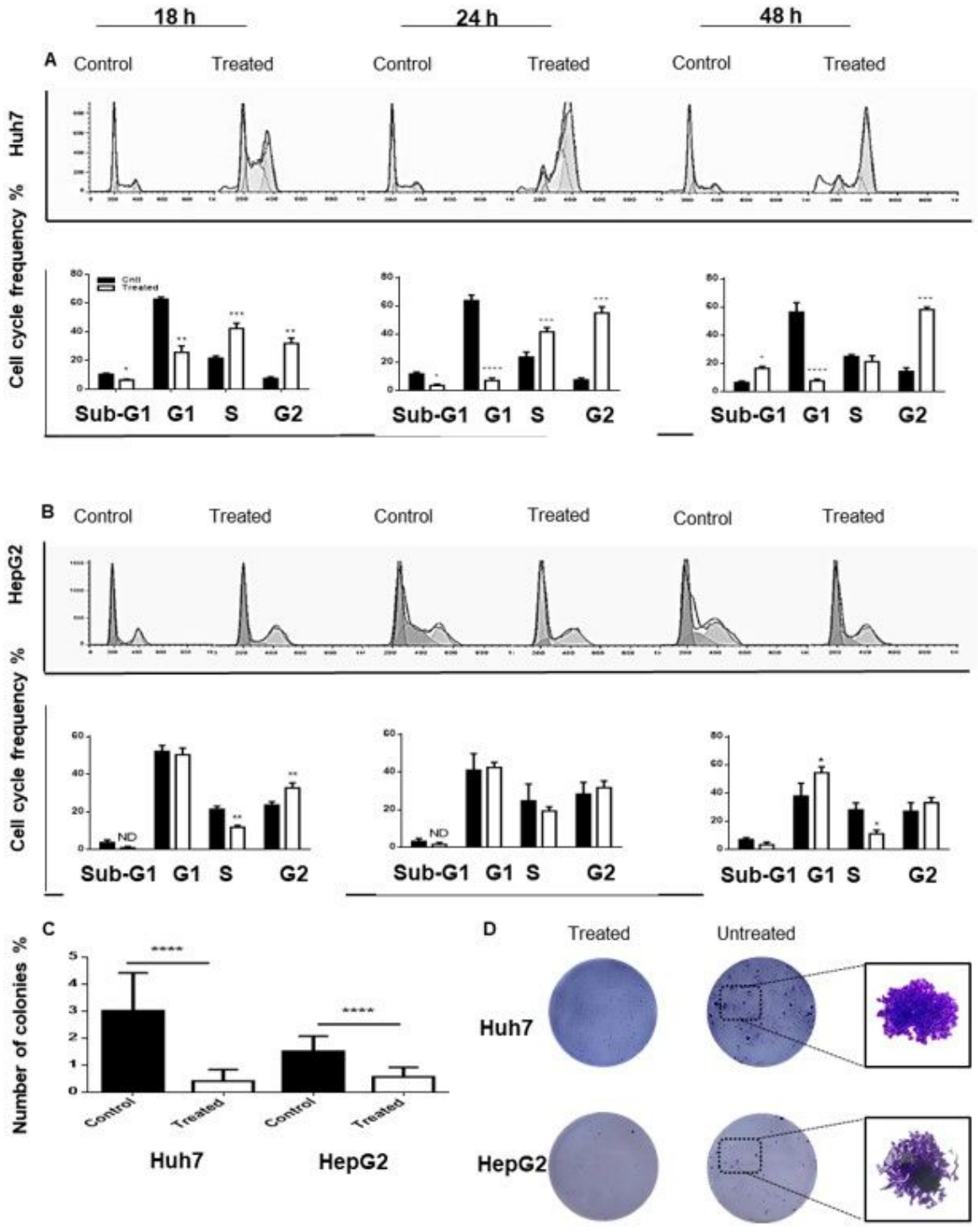

Figure 2

Cell cycle evaluation and colony formation assay. A,B, Flow cytometry evaluation of cell cycle profile for cells treated with 37 MBq (Huh7)/55 MBq (HepG2) by 188ReO4 versus untreated group after 18, 24, and

24 h post exposure using PI/ RNase staining. Data are expressed as the mean ± SD, n = 3 (* P<0.05, ** P<0.001, *** P<0.0001) versus control group. C,D. Treated cells with 37 MBq (Huh7)/55 MBq (HepG2) of 188ReO4 reduced colony formation capacity. Data are expressed as the mean ± SD, n = 3 (* P<0.05, ** P<0.001, *** P<0.0001) versus control..

Figure 3

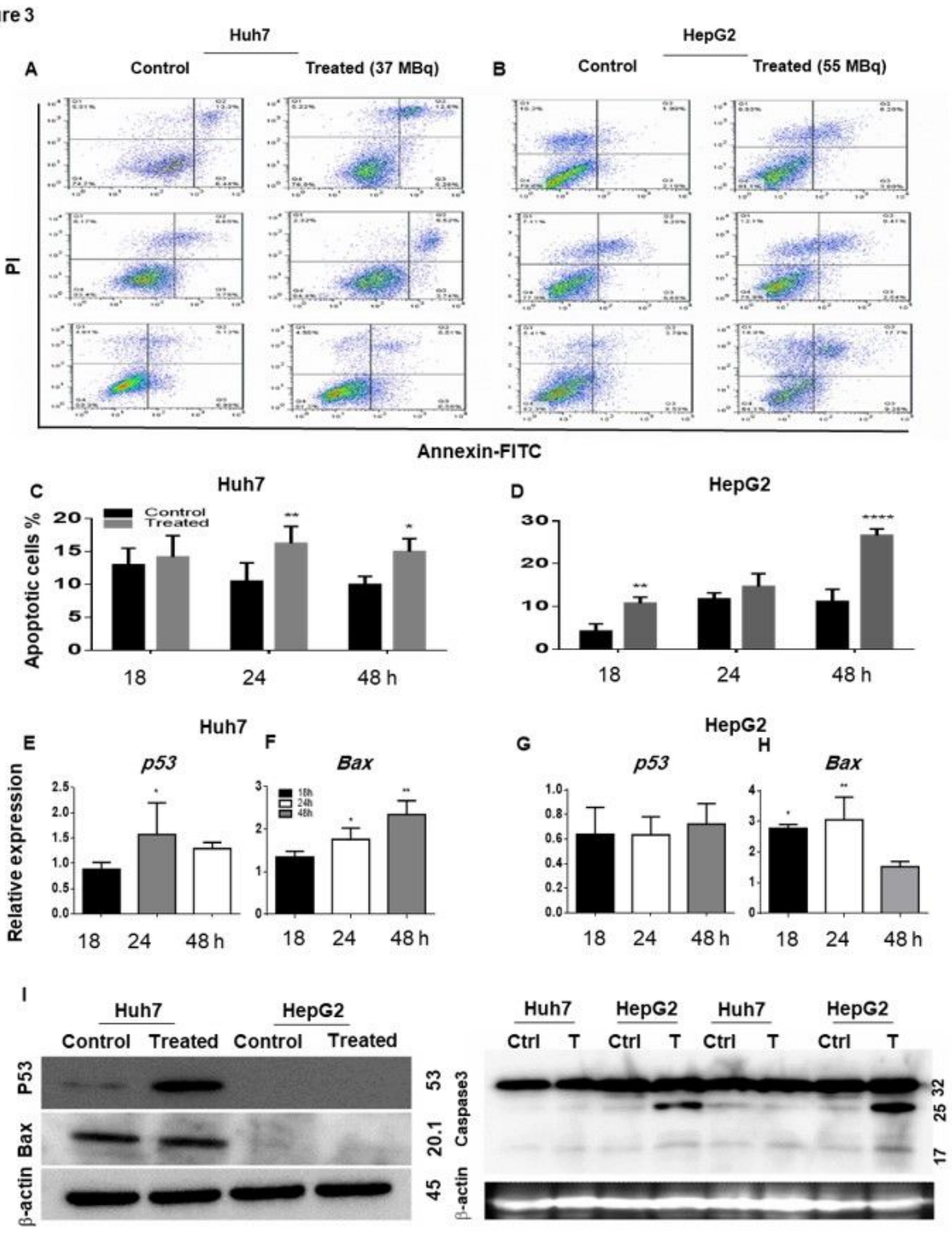

Figure 3

Apoptosis induction evaluation. A,B. Apoptosis evaluation using Anexin PI. C,D. Bar plots to show the present of apoptotic cells. E,F. The qPCR results for p53 and Bax relative mRNA expression in Huh7 and HepG2 cells treated with 37 MBq and 55 MBq of 188ReO4 versus control after 18, 24, and 48 hours post exposure. Values are presented as mean ± SD, n =3 (* P<0.05, ** P<0.001, *** P<0.0001). G,H,I. Western blots and relative bar graphs of p53 and BAX protein in Huh7 and HepG2 cells after treatment. Data are expressed as the mean ± SD, n = 3 (* P<0.05, ** P<0.001, *** P<0.0001).

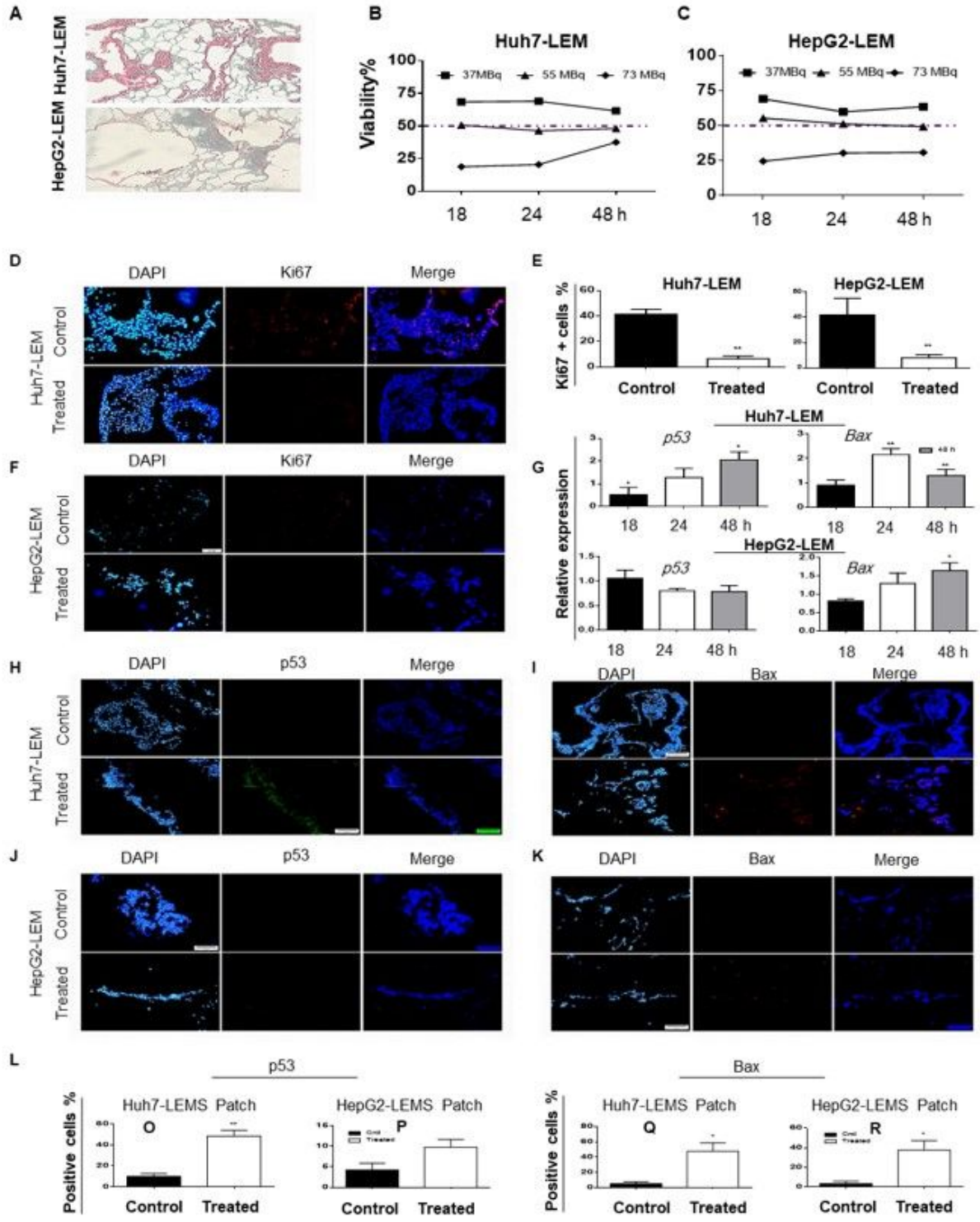

Figure 4

Evaluation of cells in 3D LEM culture. A: MT staining of Huh7 and HepG2 cells homing at synthesized LEM. B,C. Viability percent versus control for finding effective dose of 188ReO4 in Huh7/HepG2-LEM treated with 37, 55, and 73 MBq doses after 18, 24 and 48 h post exposure. D,E,F. The Ki67 positive cells representing proliferating fraction of Huh7/HepG2- LEMs that treated with 188ReO4. G. The qPCR results for p53 and Bax relative mRNA expression in Huh7/HepG2-LEMs treated with 188ReO4 versus control after 18, 24, and 48 h. Values are presented as mean ± SD, n=3; * (* $P<0.05$, ** $P<0.001$, *** $P<0.0001$) . H,I,J,Kand L. IF staining to visualize p53 and Bax protein expressions in Huh7- LEM and HepG2-LEM that treated with 188ReO4.

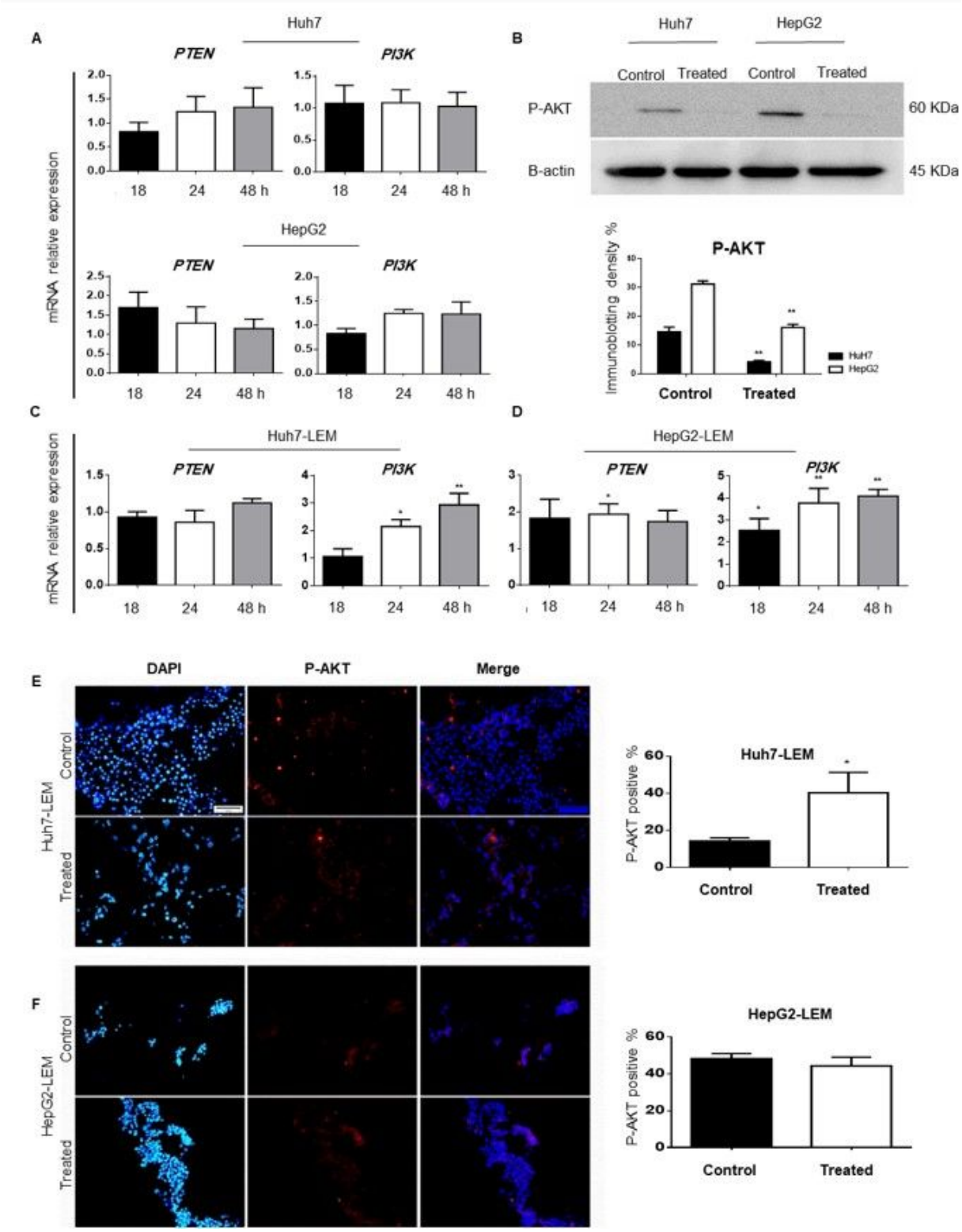

Figure 5

Radio-resistance evaluation. A, B. The qPCR results for PTEN and PI3K relative mRNA expressions in 2D cultured Huh7 and HepG2 cells treated with 37, and 55 MBq of 188ReO4 respectively versus control after 18, 24, and 48 h post exposure. Values are expressed as mean ± SD, n=3; (* P<0.05, ** P<0.001, *** P<0.0001). C,D. Western blots and relative bar graphs of P-AKT protein alternation in Huh7 and HepG2 cells, respectively after exposure versus untreated control group. Data are presented as the mean ± SD, n

= 3; (* p<0.05, ** p<0.001, *** p<0.0001) versus control group. E,F. The qPCR results for PTEN and PI3K relative mRNA expression in Huh7/HepG2-LEMs 3D culture after 18, 24, and 48 hours post exposure. Values are expressed as mean ± SD, n=3 (* P<0.05, ** P<0.001, *** P<0.0001). G,H. IF staining to detect P-AKT expression in Huh7-LEM and HepG2-LEM treated with 55 MBq of 188ReO4.

Supplementary Files

This is a list of supplementary files associated with this preprint. Click to download.

- SupplementaryFigure.docx